Primeval very low-mass stars and brown dwarfs – III. The halo transitional brown dwarfs

Z. H. Zhang (张曾华),[1,2,3]⋆† D. J. Pinfield,[4]⋆ M. C. Gálvez-Ortiz,[5] D. Homeier,[6]
A. J. Burgasser,[7] N. Lodieu,[2,3] E. L. Martín,[5] M. R. Zapatero Osorio,[5] F. Allard,[8]
H. R. A. Jones,[4] R. L. Smart,[9] B. López Martí,[10] B. Burningham[4] and R. Rebolo[2,3]

[1]*GEPI, Observatoire de Paris, Université PSL, CNRS, 5 Place Jules Janssen, F-92190 Meudon, France*
[2]*Instituto de Astrofísica de Canarias, E-38205 La Laguna, Tenerife, Spain*
[3]*Universidad de La Laguna, Dept. Astrofísica, E-38206 La Laguna, Tenerife, Spain*
[4]*Centre for Astrophysics Research, Science and Technology Research Institute, University of Hertfordshire, Hatfield AL10 9AB, UK*
[5]*Centro de Astrobiología (CSIC-INTA), Ctra. Ajalvir km 4, E-28850 Torrejón de Ardoz, Madrid, Spain*
[6]*Zentrum für Astronomie der Universität Heidelberg, Landessternwarte, Königstuhl 12, D-69117 Heidelberg, Germany*
[7]*Center for Astrophysics and Space Science, University of California San Diego, La Jolla, CA 92093, USA*
[8]*Univ Lyon, ENS de Lyon, Univ Lyon 1, CNRS, Centre de Recherche Astrophysique de Lyon, UMR5574, F-69007, Lyon, France*
[9]*Istituto Nazionale di Astrofisica, Osservatorio Astronomico di Torino, Strada Osservatrio 20, I-10025 Pino Torinese, Italy*
[10]*Saint Louis University - Madrid Campus, Avenida del Valle 34, E-28003 Madrid, Spain*

ABSTRACT

We report the discovery of an esdL3 subdwarf, ULAS J020858.62+020657.0, and a usdL4.5 subdwarf, ULAS J230711.01+014447.1. They were identified as L subdwarfs by optical spectra obtained with the Gran Telescopio Canarias, and followed up by optical-to-near-infrared spectroscopy with the Very Large Telescope. We also obtained an optical-to-near-infrared spectrum of a previously known L subdwarf, ULAS J135058.85+081506.8, and reclassified it as a usdL3 subdwarf. These three objects all have typical halo kinematics. They have $T_{\rm eff}$ around 2050–2250 K, $-1.8 \leq$ [Fe/H] ≤ -1.5, and mass around 0.0822–0.0833 M$_\odot$, according to model spectral fitting and evolutionary models. These sources are likely halo transitional brown dwarfs with unsteady hydrogen fusion, as their masses are just below the hydrogen-burning minimum mass, which is ~ 0.0845 M$_\odot$ at [Fe/H] $= -1.6$ and ~ 0.0855 M$_\odot$ at [Fe/H] $= -1.8$. Including these, there are now nine objects in the 'halo brown dwarf transition zone', which is a 'substellar subdwarf gap' that spans a wide temperature range within a narrow mass range of the substellar population.

Key words: brown dwarfs – stars: chemically peculiar – stars: individual: ULAS J020858.62+020657.0, ULAS J135058.85+081506.8, ULAS J230711.01+014447.1 – stars: Population II – subdwarfs.

1 INTRODUCTION

The formation of brown dwarfs that have masses below the hydrogen-burning minimum mass (HBMM) was predicted over a half century ago (Kumar 1963; Hayashi & Nakano 1963). Modern evolutionary models indicate that the HBMMs are between 0.07 and 0.092M$_\odot$ from solar to primordial metallicity (Baraffe et al.

2015; Burrows et al. 2001). One of the motivations to find these brown dwarfs was the potential of a new celestial population with masses between stars and planets to test stellar/substellar formation theory.

A few thousand ultracool dwarfs have been identified spectroscopically since the 1990s. To better understand the physics of stellar nuclear ignition and the inner structure of objects across the stellar–substellar boundary (Chabrier & Baraffe 1997), it is crucial to distinguish between stars and brown dwarfs with mass around the HBMM. However, evolution leads to mass/age degeneracy when considering the luminosity and effective temperature ($T_{\rm eff}$) of very low-mass star and brown dwarf populations. Therefore, it takes a

lot of effort to assess the substellar status of field ultracool dwarfs near the HBMM (e.g. Dieterich et al. 2014; Dupuy & Liu 2017).

Brown dwarfs in the thick disc and halo have a lower level of mass/age degeneracy than those in the thin disc, as they have similar ages to the stellar populations in the thick disc (∼8–10 Gyr; Reddy, Lambert, & Allende Prieto 2006; Kilic et al. 2017) and the halo (∼10–13 Gyr; Dotter et al. 2010; Jofré & Weiss 2011) and they have evolved to a stage with slowed-down of cooling. However, they are distributed in a wide range of metallicity and have different HBMMs at different metallicities. Therefore, the metallicity measurements offer significant scope to tackle the mass/metallicity degeneracy problem for thick-disc and halo brown dwarfs.

In the first paper of a series under the title 'Primeval very low-mass stars and brown dwarfs', we defined a new classification scheme for L subdwarfs and characterized a sample of 22 metal-deficient ultracool subdwarfs (Zhang et al. 2017a, hereafter Paper I). In the second paper of the series, we assessed the stellar–substellar boundary in the $T_{\rm eff}$ versus [Fe/H] plane based on theoretical model prediction of the HBMM (Zhang et al. 2017b, hereafter Paper II). This provided an alternative method to assess substellar status for nearby ultracool subdwarfs, and revealed a 'halo brown dwarf transition zone' representing a narrow mass range in which unsteady nuclear fusion occurs – a 'substellar subdwarf gap' for mid L to early T types. Currently, there are six L subdwarfs known in this transition zone: SDSS J010448.46+153501.8 (Lodieu et al. 2017; Paper II), 2MASS J05325346+8246465 (Burgasser et al. 2003), 2MASS J06164006−6407194 (2M0616; Cushing et al. 2009), SDSS J125637.13−022452.4 (SD1256; Sivarani et al. 2009), ULAS J151913.03−000030.0 (UL1519; Paper I), and 2MASS J16262034+3925190 (2M1626; Burgasser 2004a).

This is the third paper of the series following Paper I and Paper II, in which we grow the halo transitional brown dwarf population further, presenting the discovery of three new members. The observations are presented in Section 2. Section 3 presents constraints on the physical characteristics of these objects. Finally Section 4 presents a summary and conclusions.

2 OBSERVATIONS

ULAS J020858.62+020657.0 (UL0208) and ULAS J230711.01+014447.1 (UL2307) were selected as L subdwarf candidates from the UKIRT Infrared Deep Sky Survey's (UKIDSS; Lawrence et al. 2007) Large Area Survey (LAS) and the Sloan Digital Sky Survey (SDSS; York et al. 2000). The selection criteria and procedure are described in Paper I. The properties of UL0208 and UL2307 are summarized in Table 1. The spectroscopic observations are summarized in Table 2.

2.1 GTC spectroscopy

UL0208 and UL2307 were first identified as L subdwarfs by their optical spectra obtained with the Optical System for Imaging and low Resolution Integrated Spectroscopy (OSIRIS; Cepa et al. 2000) instrument on the Gran Telescopio Canarias (GTC). An R500R grism and 0.8 arcsec slit were used for observations of UL0208 and UL2307, which provide a resolving power of ∼500 and cover a wavelength range of 480–1020nm. These spectra were reduced

Table 1. Properties of UL0208, UL1350, and UL2307.

Parameter	UL0208	UL1350	UL2307
α (J2000)	$02^{\rm h}08^{\rm m}58\overset{\rm s}{.}62$	$13^{\rm h}50^{\rm m}58\overset{\rm s}{.}85$	$23^{\rm h}07^{\rm m}11\overset{\rm s}{.}01$
δ (J2000)	$+02°06'57\overset{''}{.}0$	$+08°15'06\overset{''}{.}8$	$+01°44'47\overset{''}{.}1$
Epoch	2010-08-28	2006-07-08	2009-08-11
SDSS i	21.54 ± 0.07	21.22 ± 0.08	22.53 ± 0.22
SDSS z	19.86 ± 0.07	19.47 ± 0.06	19.91 ± 0.09
PS1 i	21.39 ± 0.03	21.14 ± 0.07	21.69 ± 0.16
PS1 z	19.99 ± 0.03	19.68 ± 0.05	20.16 ± 0.04
PS1 y	19.50 ± 0.06	19.32 ± 0.04	19.57 ± 0.08
UKIDSS Y	18.76 ± 0.05	18.66 ± 0.05	18.99 ± 0.08
UKIDSS J	18.00 ± 0.04	17.93 ± 0.04	18.15 ± 0.06
UKIDSS H	17.88 ± 0.13	18.07 ± 0.10	18.34 ± 0.12
UKIDSS K	17.62 ± 0.16	17.95 ± 0.15	18.17 ± 0.18
Spectral type	esdL3 $\pm$ 1	usdL3 $\pm$ 1	usdL4.5 $\pm$ 1
Distance (pc)	171^{+32}_{-27}	176^{+25}_{-22}	157^{+19}_{-18}
$\mu_{\rm RA}$(mas yr^{-1})	147.1 ± 8.4	-252.8 ± 5.4	-33.0 ± 9.1
$\mu_{\rm Dec}$(mas yr^{-1})	-143.1 ± 10.4	-248.5 ± 4.3	-202.6 ± 2.6
$V_{\rm tan}$ (km s^{-1})	166 ± 31	239 ± 39	205 ± 30
Radial velocity (km s^{-1})	52 ± 10	58 ± 9	-215 ± 11
U (km s^{-1})	-58 ± 27	-23 ± 26	67 ± 41
V (km s^{-1})	-151 ± 50	-299 ± 88	-232 ± 48
W (km s^{-1})	-64 ± 28	33 ± 28	106 ± 40
$T_{\rm eff}$ (K)	2250 ± 120	2250 ± 120	2050 ± 120
[Fe/H]	-1.5 ± 0.2	-1.8 ± 0.2	-1.7 ± 0.2
M (per cent M$_\odot$)	8.27 ± 0.15	8.33 ± 0.15	8.22 ± 0.15

using standard procedures within IRAF.[1] Standard stars G158−100 (dG-K; Oke 1990) and GD140 (DA WD; Massey et al. 1988) were used for the flux calibration of UL0208 and UL2307, respectively. The contamination from the second-order filter is not corrected for standard stars; therefore, the flux calibration beyond 900 nm is based on the extension of the first-order response function and somewhat uncertain. However, the flux of these OSIRIS spectra are roughly consistent with their X-shooter spectra (we obtained later) at 900–1020 nm except the telluric region at 925–965 nm. Telluric is not corrected for these OSIRIS spectra. The signal-to-noise ratio (SNR) at 850 nm is ∼60 and ∼55 for the spectra of UL0208 and UL2307, respectively.

2.2 VLT spectroscopy

UL0208 and UL2307 were followed up with the X-shooter spectrograph (Vernet et al. 2011) on the Very Large Telescope (VLT) of the European Southern Observatory (ESO), together with another previously known L subdwarf, ULAS J135058.85+081506.8 (UL1350; Lodieu et al. 2010, 2017). We also observed an L0.5 dwarf radial velocity (RV) standard, DENIS-P J144137.3−094559 (DE1441; Martín et al. 1999; Bailer-Jones 2004) with X-shooter for RV measurements of our objects. All X-shooter spectra were observed in an ABBA nodding mode with a 1.2 arcsec slit providing a resolving power of 6700 in the visible (VIS) arm (530–1020 nm) and 4000 in the near-infrared (NIR) arm (990–2480 nm). These spectra were reduced to flux- and wavelength-calibrated 2D spectra with ESO Reflex (Freudling et al. 2013). The 1D spectra were extracted from these 2D spectra using the IRAF task APSUM. Telluric corrections

---

[1] IRAF is distributed by the National Optical Observatory, which is operated by the Association of Universities for Research in Astronomy, Inc., under contract with the National Science Foundation.

Table 2. Summary of the spectroscopic observations.

Name	Telescope	Instrument	UT date	Seeing ($''$)	Airmass	T_{int}(VIS) (s)	T_{int}(NIR) (s)	Telluric star	SpT	Airmass
UL0208	GTC	OSIRIS	2013-09-09	0.80	1.76	2700	–	–	–	–
UL2307	GTC	OSIRIS	2013-07-05	0.80	1.27	3600	–	–	–	–
UL0208	VLT	X-shooter	2014-11-29	1.13	1.13	3384	3480	HD 22686	A0 V	1.14
UL2307	VLT	X-shooter	2015-09-11	1.02	1.13	3420	3600	HIP 105164	B7 III	1.09
UL1350	VLT	X-shooter	2016-03-22	0.59	1.20	3480	3600	HIP 79439	B9 V	1.42
DE1441	VLT	X-shooter	2016-03-19	0.66	1.11	1120	1200	HIP 76836	B9.5 V	1.11

were achieved using telluric standards which were observed right after or before our targets at a very close airmass.

The spectrum of UL0208 has an SNR (per pixel) of ∼3 at 830 nm and ∼6 at 1300 nm. The spectrum of UL2307 has an SNR of ∼5 at 830 and 1300 nm. The spectrum of UL1350 has an SNR of ∼6 at 830 and 1300 nm. These spectra presented in this paper have a resolving power of ∼600 as they were smoothed by 101 pixels and 51 pixels for the VIS and NIR arms to increase the SNR by factors of ∼10 and ∼7, respectively. The spectrum of the DE1441 has an SNR of ∼20 at 830 nm and ∼70 at 1300 nm.

3 CHARACTERISTICS

3.1 Spectral classification

We classify UL0208, UL2307, and UL1350 following our L subdwarf classification scheme (Paper I). L subdwarfs are classified into three metallicity subclasses, subdwarf (sdL), extreme subdwarf (esdL), and ultra-subdwarf (usdL), based on their optical-to-NIR spectra. The classification scheme was set up such that the subclass sequence follows a decreasing trend in metallicity. The overall profiles of L subdwarfs respond to both T_{eff} and metallicity. The overall optical-to-infrared spectral energy distribution becomes bluer for both warmer T_{eff} and/or lower metallicity; however, features such as the 705–730 and 840–860 nm TiO bands are specifically metal-sensitive (see table 3 in Paper I).

The population of known L subdwarfs with good-quality optical-to-NIR spectra does not fully populate every subclass/subtype in the scheme, so we followed a two-stage approach. First, we compared our target spectra to those of the available classified subdwarfs and identified objects that provided a reasonable match (in terms of overall morphology and important spectral features). Then we considered each match in more detail, and made decisions about optimal choice and any intermediate classifications.

There were four classified subdwarfs (with good optical-to-NIR spectra) that gave reasonable matches to our three objects. These were the esdL6 2M0616 (Cushing et al. 2009), the usdL3 SD1256 (Sivarani et al. 2009), the esdL4 UL1519 (Paper I), and the usdL4 2M1626 (Burgasser 2004a). Figs 1 and 2 show the optical and NIR spectra of our objects (UL0208, UL2307, and UL1350) compared to those of the four classified L subdwarfs.

As can be seen, UL0208 has a similar optical spectrum to the usdL3 SD1256; however, it has slightly less flux at 720–770 nm, indicating a higher metallicity. Also, compared to the esdL UL1519, UL0208 has slightly more flux at 780–810 nm, weaker TiO absorption at around 840–860 nm, and stronger NIR suppression, indicating a slightly lower metallicity than UL1519. Comparison between the optical spectra of UL0208 and 2M1626 shows that UL0208 has an earlier spectral type (SpT) than 2M1626. Therefore, we classify UL0208 as an esdL3 subdwarf.

The optical spectrum of UL2307 appears to be intermediate between those of the usdL4 2M1626 and the esdL6 2M0616 (see Fig. 1). However, its NIR spectrum is significantly more suppressed than that of these subdwarfs, with an overall optical-to-NIR morphology that is closer to 2M1626 than to 2M0616. We therefore assign UL2307 the same subclass as 2M1626. Having said this, UL2307 has slightly less flux in the optical and slightly more flux in the NIR compared to 2M1626, which leads us to assign it a slightly later subtype. We classified UL2307 as a usdL4.5 subdwarf.

Fig. 1 shows that both UL0208 and Ul2307 have very different optical spectral features (e.g. TiO) from the standard L3 dwarf DENIS-P J1058.7−1548 (DE1058; Delfosse et al. 1997; Kirkpatrick et al. 1999) and L4.5 dwarf 2MASS J2224438−015853 (2M2224; Kirkpatrick et al. 2000) because of their much lower metallicity. Metallicity has a stronger influence on the spectral profile of L subdwarfs in the NIR than in the optical (e.g. fig. 9 in Paper I).

UL1350 was originally classified as sdL5 by Lodieu et al. (2010) based on a low SNR optical spectrum, but was then re-classified sdL3.5–4 based on an improved SNR optical spectrum (Lodieu et al. 2017). In Paper I, we suggested that UL1350 should have the same spectral type as SD1256 (usdL3). And here we are now able to assess the full optical–NIR spectra. These spectra (shown in Figs 1 and 2) show that UL1350 has an optical-to-NIR morphology that is very similar to SD1256, and we thus classify UL1350 as usdL3.

3.2 Halo kinematics

We derived spectroscopic distance estimates for UL0208, UL1350, and UL2307 using the relationship between spectral type and *J*- and *H*-band absolute magnitude shown in fig. 16 of Paper I. We computed distances using both *J*- and *H*-band magnitudes, which for all three sources agreed within the uncertainties; the average distances are listed in Table 1. Upper and lower limits were determined by considering the *J*- and *H*-band constraints, and positive and negative error bars were assigned for each object.

Proper motions were determined using multi-epoch optical and NIR data. UL0208, UL1350, and UL2307 were observed by SDSS on 2009 September 27, 2003 April 27, and 2008 October 02, respectively. They were subsequently observed by UKIDSS and Pan-STARRS1 (PS1; Chambers et al. 2016). Multi-epoch PS1 images of each target were combined, with mean epochs of 2012 July 31, 2011 March 12, and 2012 October 23, for UL0208, UL1350, and UL2307 respectively. The proper motions of UL0208 and UL1350 were measured using SDSS *z*- and PS1 *z*-band images that had baselines of 2.84 and 7.88 yr, respectively, following the method described in section 3.2 of Paper II. The proper motion of UL2307 was measured from PS1 *z*- and UKIDSS *J*-band images which provided a baseline of 3.20 yr. The numbers of reference stars used for proper motion measurements were 22, 9, and 9 for UL0208,
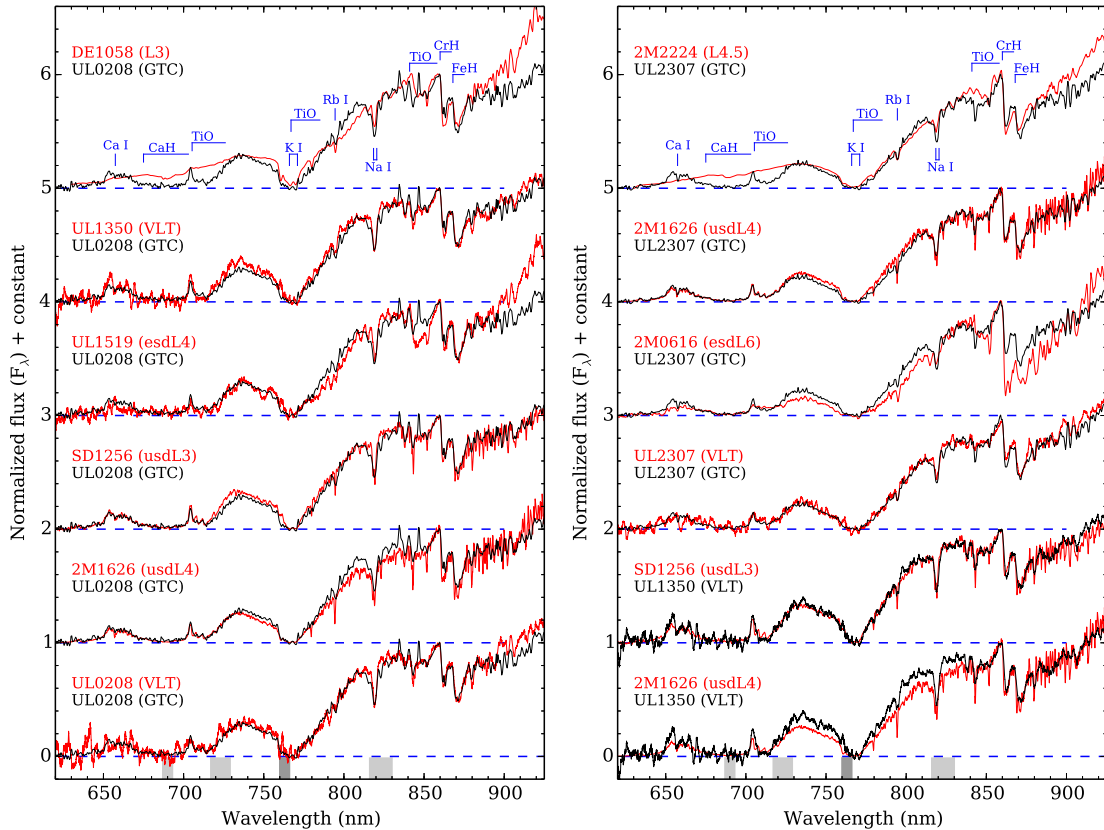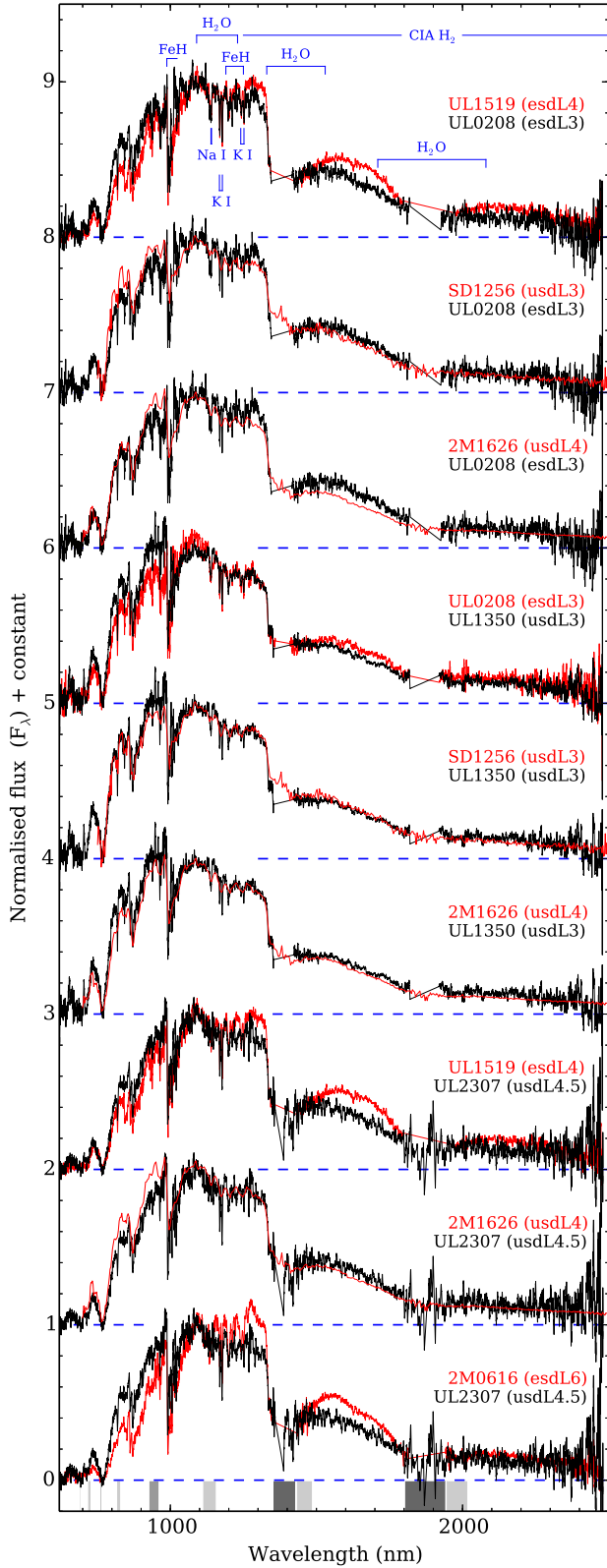
Figure 1. The optical spectra of UL0208, UL1350, and UL2307, compared to spectra of known objects from Burgasser et al. (2009, SD1256); Burgasser, Cruz, & Kirkpatrick (2007, 2M1626); Paper I (UL1519); Cushing et al. (2009, 2M0616); Kirkpatrick et al. (1999, DE1058); and Kirkpatrick et al. (2000, 2M2224). Spectra are normalized near 860 nm. Telluric absorption wavelengths are indicated with grey strips at the bottom and have been corrected for our VLT spectra, but not for our GTC spectra. Lighter and thicker shaded bands indicate regions with weaker and stronger telluric effects.

UL1350, and UL2307, respectively. Our measured proper motions are listed in Table 1.

We measured RVs for UL0208, UL2307 and UL1350 by cross correlation of their X-shooter optical and NIR spectra to that of an DE1441 which has a RV of $-27.9 \pm 1.2\,\mathrm{km\,s^{-1}}$ (Bailer-Jones 2004). We smoothed our original X-shooter spectra by 21 pixels in the VIS and 11 pixels in the NIR to increase the SNR. The RV differences between our objects and the standard were measured with the IRAF task FXCOR. Then the RVs were corrected for the barycentric effects. The final RVs of UL0208, UL2307, and UL1350 are listed in Table 1.

The Galactic *UVW* space motions of UL0208, UL2307, and UL1350 were determined using our spectroscopic distances, RVs, and proper motions following Clarke et al. (2010). The resulting *U*, *V*, and *W* velocities are listed in Table 1. UL0208, UL2307, and UL1350 have typical halo kinematics (see fig. 17 of Paper I), in keeping with their low metallicity making them halo members with ages of ∼10–13 Gyr (Dotter et al. 2010; Jofré & Weiss 2011).

We calculated the halo membership probabilities of these three objects based on kinematics and population fractions of thin-disc (0.93), thick-disc (0.07), and halo (0.006) stars in the solar neighbourhood (Reddy et al. 2006). UL1350 and UL2307 have halo membership probabilities of 99.9 per cent and 99.1 per cent, respectively. UL0208 has a higher thick-disc probability (82.9 per cent) and a lower halo probability (17.1 per cent), as the thick-disc fraction is ∼10 times higher than the halo fraction. UL0208 would have a halo probability of 70.1 per cent if we applied an equal fraction of

halo and thick-disc populations in the calculation. The halo membership of UL0208 becomes robust when considering its typical halo metallicity of [Fe/H] = −1.5.

3.3 Atmospheric properties

We used the BT-Dusty models (Allard, Homeier, & Freytag 2014) to constrain the atmospheric parameters of UL0208, UL1350, and UL2307. The model grids we used cover 1900 K $\leqslant T_{\mathrm{eff}} \leqslant$ 3500 K, $-2.5 \leqslant$ [Fe/H] $\leqslant -1.0$, and $5.0 \leqslant \log g \leqslant 5.5$, with intervals of 100 K for T_{eff}, 0.5 dex for [Fe/H], and 0.5 dex for $\log g$. Linear interpolation between some model spectra was used if this yielded a significantly improved fit. We followed the procedure described in section 3.3 of Paper II to find best-fitting model spectra to our sources.

Fig. 3 shows the optical and NIR spectra of UL0208, Ul1350, and UL2307 compared to their best-fitting models. These best-fitting models have T_{eff} = 2250 K and [Fe/H] = −1.5 for UL0208; T_{eff} = 2250 K and [Fe/H] = −1.8 for UL1350; T_{eff} = 2050 K and [Fe/H] = −1.7 for UL2307. All these models have gravity of $\log g$ = 5.50 and α enhancement of [α/Fe] = +0.4. These model spectra in general provide a very good fit to the data with the exception of the 840–880 nm region, where the TiO, CrH, and FeH absorption bands are less well fitted.

We have combined our new T_{eff} values with those from Paper I and Paper II, and extended this sample with an additional 50 K6.5–M5.5 subdwarfs in the $-2.0 \leqslant$ [Fe/H] $\leqslant -1.0$ range. Using
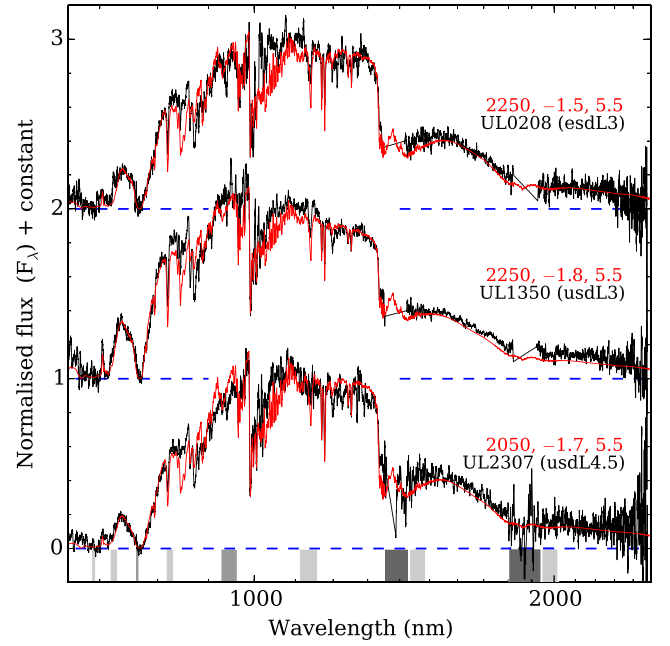
Figure 3. The optical–NIR X-shooter spectra of UL0208, UL1350, and UL2307 obtained with the VLT, compared to their best fitting BT-Dusty model spectra. T_{eff}, [Fe/H], and log g values for each model are indicated next to the spectra. Spectra are normalized at 1100 nm. The axis tick marks are spaced logarithmically to more clearly display the features of the optical spectra.

this sample, we have updated the polynomial fit for the relationship between ultracool subdwarf SpT and T_{eff}, which follows:

$$T_{eff} = 3701 - 108.6 \times SpT + 1.855 \times SpT^2 - 0.1661 \times SpT^3 \quad (1)$$

with a root mean square (rms) of 32 K. In this equation SpT = −1 for K7, SpT = 0 for M0, SpT = 10 for L0, and SpT = 15 for L5 (etc). Equation (1) is valid for K7–L7 subdwarfs with [Fe/H] $\lesssim$ −1.0.

Fig. 4 shows the SpT–T_{eff} relationships of dwarf populations with different metallicities. Objects with lower metallicity tend to have lower T_{eff} before M3 and higher T_{eff} from M5 to L7 types. M6–L7 subdwarfs with [Fe/H] $\leqslant$ −1.0 are ∼200–400 K warmer than field dwarfs. The SpT–T_{eff} relation for young L dwarfs is in general somewhat cooler (by ∼200 K) than the field relation, and is thus offset in the opposite sense to the subdwarf fit. The large difference between these SpT–T_{eff} relationships is due to different SpT–mass correlations, opacities, and ages of these populations. A metal-poor star would have a lower opacity, higher T_{eff}, and bluer spectral continuum than a solar-metallicity star with the same mass, and thus could have the same spectral subtype as more massive stars with higher metallicities (fig. 9; Paper II). Dwarf stars have higher mass than subdwarfs with the same spectral type before ∼M6 and a sharper mass decline from M3 to M5 types (Mann et al. 2015). Then subdwarfs start to have higher masses from M7 to L types. Meanwhile, young ultracool dwarfs have much lower masses than field objects but retain a warm T_{eff} at young ages.

3.4 Halo transitional brown dwarfs

Evolutionary models (Baraffe et al. 1997; Chabrier & Baraffe 1997; Burrows et al. 1998) show that there is a halo brown dwarf transition zone in a T_{eff} versus [Fe/H] plane, which is between ∼1200 K and

Figure 2. The optical–NIR spectra of UL0208, UL1350, and UL2307 compared to spectra of known objects from Burgasser et al. (2009, SD1256); Burgasser (2004a, 2M1626); and Paper I (UL1519 and 2M0616). Spectra are normalized near 1100 nm.
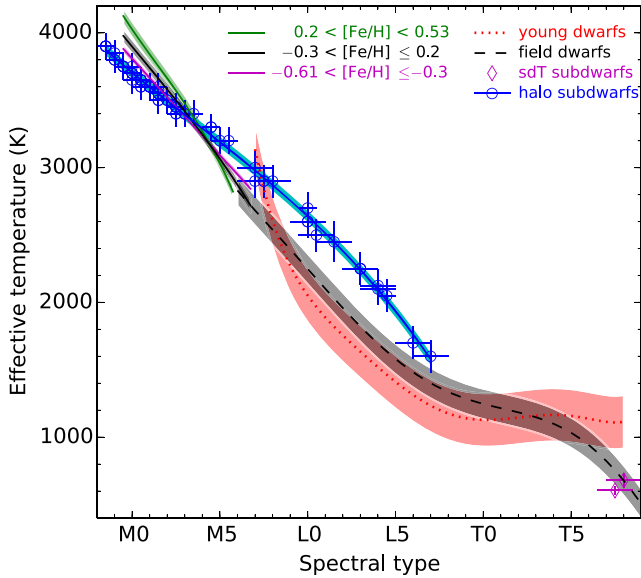
Figure 4. The correlation between spectral type and T_{eff}. The blue solid, black dashed, and red dotted lines are for halo subdwarfs, field dwarfs (Filippazzo et al. 2015), and young dwarfs (Faherty et al. 2016), respectively. The green, black, and magenta solid lines are for M dwarfs in different metallicity ranges (Mann et al. 2015). Two magenta diamonds indicate two sdT subdwarfs: BD+01° 2920 B (Pinfield et al. 2012) and ULAS 1416+1348 (Line et al. 2017).

Figure 5. Six known (blue squares) and three new (red circles) halo transitional brown dwarfs plotted in a [Fe/H] and T_{eff} space. Black solid and dashed (interpolated) lines indicate the 10 Gyr iso-mass contours derived from evolutionary models (Baraffe et al. 1997; Chabrier & Baraffe 1997). Magenta solid lines are 10 Gyr iso-mass contours based on calculations of Burrows et al. (1998). The mass value (in $M_\odot$) is marked next to each iso-mass line. Note that the accuracy of these iso-mass contours is related to the density of the metallicity grid. The green line indicates the stellar–substellar boundary (Paper II). T_{eff} of solar-metallicity objects at 10 Gyr predicated by Baraffe et al. (2003, 2015) are joined with those of metal-poor models (with corresponding mass) by black and red dotted lines, respectively. These black dotted lines above [Fe/H] = −0.6 are not representing the true T_{eff} of thin- and thick-disc brown dwarfs with corresponding masses, because stars with [Fe/H] ≳ −0.6 usually have age ≲ 8 Gyr (Reddy et al. 2006).

the corresponding T_{eff} (∼2200–3000 K) of the HBMM at different metallicities (Paper II). Six L subdwarfs have previously been identified as members of this transition zone. They are supported by electron degeneracy, and unsteady nuclear ignition takes place in their cores, but they cannot balance ongoing gravitational contraction. These halo transitional brown dwarfs are fully convective and could sporadically reach states of minimum temperature and pressure in their cores to fuse hydrogen. The unsteady hydrogen fusion in halo transitional brown dwarfs is less efficient and could last longer than the steady hydrogen fusion in least-massive stars which would have a main sequence lifetime of ∼12 trillion years (Adams, Bodenheimer, & Laughlin 2005).

The unsteady hydrogen fusion partially contributed to the luminosities of halo transitional brown dwarfs. Burgasser et al. (2008) show that around half of the luminosity of 2MASS J05325346+8246465 is generated from its core hydrogen fusion at 10 Gyr. The efficiency (intensity or frequency) of the unsteady sporadic hydrogen fusion is sensitive to the masses of transitional brown dwarfs, because the halo brown dwarf transition zone covers a narrow mass range (∼90–99 per cent HBMM) but spans wide ranges of luminosity and temperature (see figs 4 and 5 in Burrows et al. 2001). For example, an object with 0.08 $M_\odot$ and [Fe/H] = −2.3 would have a $T_{eff} \approx 1200$ K; however, an object with 0.085 $M_\odot$ and the same [Fe/H] would have a $T_{eff} \approx 2400$ K (see Fig. 5).

Fig. 5 shows UL0208, UL1350, and UL2307 in the T_{eff} versus [Fe/H] plane. They lie in the halo brown dwarf transition zone joined by six previously known members, which were identified using the method described in Paper II with atmospheric properties from Paper I. Masses of these nine halo transitional objects have been estimated from their location relative to the iso-mass contours in the diagram, and are shown in Table 3. The lowest-mass stars have stable T_{eff} at 10–13 Gyr (e.g. fig 8 of Burrows et al. 2001), so the iso-mass contours and the T_{eff} values of the HBMM line in
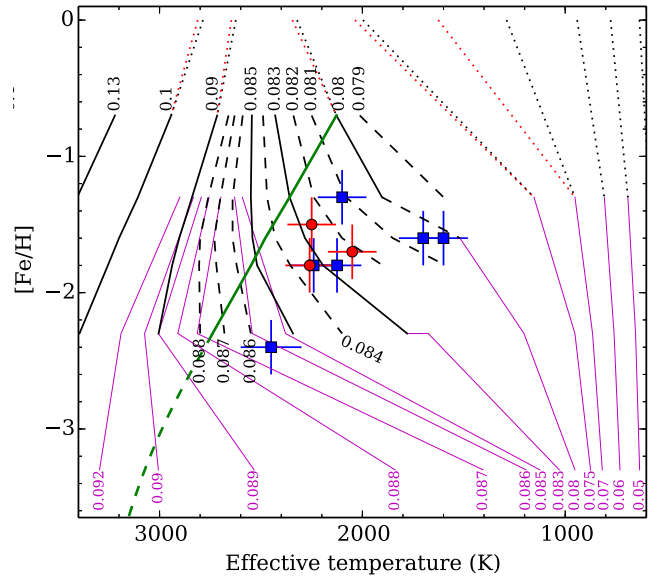
Fig. 5 are age-independent for halo stars. However, age uncertainty may affect our mass estimates for the halo brown dwarfs by up to 0.0005 $M_\odot$, because massive brown dwarf T_{eff} drops by ∼50–100 K from 10 Gyr to 11–13 Gyr (e.g. Baraffe et al. 2003). The mass uncertainty caused by T_{eff} error is around 0.001 $M_\odot$, and the mass uncertainty caused by [Fe/H] error (0.2 dex) is around 0.008–0.001 $M_\odot$. The total uncertainty based on combining in quadrature is thus 0.0015 $M_\odot$. The mass uncertainty is thus small, and is mainly due to T_{eff} uncertainty (since T_{eff} is very sensitive to mass in the halo brown dwarf transition zone, a small mass change leads to a significant change in core fusion intensity).

An sdL7 subdwarf, ULAS J133836.97−022910.7 (UL1338), has $T_{eff} = 1650\pm120$ K and [Fe/H] = −1.0 ± 0.2 (Paper I), and is a brown dwarf according to fig 9 of Paper II. However, UL1338 could belong to either the thick-disc or the halo population as its [Fe/H] is at the thick-disc/halo boundary. Furthermore, its [Fe/H] could be underestimated, since its NIR spectrum has low SNR and the [Fe/H] derived from the BT-Settl model fits is less reliable for [Fe/H] ≳ −1.0 than that for [Fe/H] < −1.0. Therefore, UL1338 currently is not listed as a halo transitional brown dwarf. VVV J12564163-6202039 (VVV1256) is a high proper motion L subdwarf identified by Smith et al. (2018). It could be either an sdL7 brown dwarf or an esdL1 star by its poor-quality optical–NIR spectrum and photometric colours. Better-quality optical–NIR spectra are required to confirm the status of VVV1256 and UL1338.

Table 3. Properties of nine known halo transitional brown dwarfs. SpT_d and Ref_d are the initial spectral type and reference. SpT_a and Ref_a are adopted spectral type (based on Paper I) and reference. Uncertainties on T_{eff}, [Fe/H], and Mass (M) are approximately 120 K, 0.2 dex, and 0.0015 $M_\odot$, respectively.

Name	SpT_d	Ref_d	SpT_a	Ref_a	T_{eff} (K)	[Fe/H]	M ($M_\odot$)
SDSS J010448.46+153501.8	sdM9.5	Lodieu et al. (2017)	usdL1.5	Paper II	2450	−2.4	0.0860
ULAS J020858.62+020657.0	–	–	esdL3	This paper	2250	−1.5	0.0827
2MASS J05325346+8246465	sdL7	Burgasser et al. (2003)	esdL7	Paper I	1600	−1.6	0.0802
2MASS J06164006−6407194	sdL5	Cushing et al. (2009)	esdL6	Paper I	1700	−1.6	0.0805
SDSS J125637.13−022452.4	sdL4	Sivarani et al. (2009)	usdL3	Paper I	2250	−1.8	0.0833
ULAS J135058.86+081506.8	sdL3.5–4	Lodieu et al. (2017)	usdL3	This paper	2250	−1.8	0.0833
ULAS J151913.03−000030.0	esdL4	Paper I	esdL4	Paper I	2100	−1.3	0.0811
2MASS J16262034+3925190	sdL4	Burgasser (2004a)	usdL4	Paper I	2125	−1.8	0.0828
ULAS J230711.01+014447.1	–	–	usdL4.5	This paper	2050	−1.7	0.0822

3.5 Lithium detection in halo brown dwarfs

Brown dwarfs with solar metallicity and mass less than ∼0.06 $M_\odot$ do not acquire core temperatures to fuse lithium ($\gtrsim$ 2.5 million K), and retain this element throughout their lives (e.g. fig 7 of Burrows et al. 2001). The lithium depletion test (Rebolo, Martin, & Magazzu 1992; Magazzu, Martin, & Rebolo 1993) is a robust method to confirm young or field degenerate brown dwarfs with mass below 0.06 $M_\odot$ (e.g. Basri, Marcy, & Graham 1996; Rebolo et al. 1996; Ruiz, Leggett, & Allard 1997; Lodieu et al. 2015b). However, this method may be incapable of confirming old halo brown dwarfs.

The maximum core temperature of a brown dwarf with 0.06 $M_\odot$ and [M/H] $\leqslant$ −1.0 is almost 0.2 million K below the minimum temperature to fuse lithium (fig. 10; Chabrier & Baraffe 1997). A core temperature difference of 0.2 million K is corresponding to a mass difference of ∼0.005 $M_\odot$ for brown dwarfs in this mass range (fig. 2; Burrows et al. 2001). Therefore, the lithium-burning minimum mass is likely around 0.065 $M_\odot$ at [M/H] $\leqslant$ −1.0. The Li line at 670.78 nm was not detected in the spectra of SD1256 and 2M1626 (Lodieu et al. 2015a). Note that their masses are ∼27 per cent higher than 0.065 $M_\odot$ (see Table 3). Halo brown dwarfs with [M/H] $\leqslant$ −1.0 (i.e. [Fe/H] $\leqslant$ −1.3) and masses below 0.065 $M_\odot$ would have T_{eff} $\lesssim$ 900 K at 10 Gyr, according to Fig. 5. Brown dwarfs with T_{eff} $\lesssim$ 900 K would have spectral types later than T5 (Fig. 4) and barely have flux at < 770 nm to unveil monatomic lines.

Lithium starts to condense into LiCl as well as LiOH and LiH in the atmospheres of brown dwarfs when temperatures drop down below ∼1525 K, and monatomic lithium decreases in abundance with decreasing temperature (Lodders 1999). Therefore, Li lines are not expected in the optical spectra of halo brown dwarfs, which could be either massive enough to fuse lithium to helium or cool enough to condense lithium into LiCl, LiOH, or LiH.

Metal hydrides (e.g. FeH) are favoured in the atmospheres of metal-poor L subdwarfs (Paper I). Shi, Stancil, & Wang (2013) also suggest that LiH might be a better candidate for detection of lithium molecules in the mid-infrared spectra of brown dwarfs than LiCl (Weck et al. 2004). Therefore, LiH might be more important than LiCl and LiOH in halo degenerate brown dwarfs, which would have insufficient metals (e.g. Cl, O) to combine with lithium.

4 SUMMARY AND CONCLUSIONS

We have presented optical and NIR spectra of two new L subdwarfs (UL0208, UL2307) and a known L subdwarf (UL1350) obtained with OSIRIS and X-shooter. We classified them as esdL3, usdL4.5, and usdL3, respectively. We measured their astrometry and kinematics, and determined their T_{eff} and [Fe/H] by fitting model spectra. We determined their mass by comparing to model iso-mass contours

in the T_{eff} versus [Fe/H] plane and found that these three objects all have masses below the HBMMs at their metallicities. They therefore join a population of nine halo transitional brown dwarfs known to date, which we summarize in Table 3.

The unsteady core hydrogen fusion in halo transitional brown dwarfs partially contributed to their luminosities and helped them to maintain intermediate luminosities and T_{eff} between least-massive stars and degenerate brown dwarfs. Halo transitional brown dwarfs are distributed in a T_{eff} range wider than 1000 K within a narrow mass range and naturally form a 'substellar subdwarf gap'. Objects in this gap have a maximum mass relative difference of ∼10 per cent and a maximum T_{eff} relative difference of ∼2.5 times. Note that a substellar gap would not be distinctly revealed by luminosity or T_{eff} among field dwarf populations, as field transitional brown dwarfs have a relatively shorter cooling time (narrower T_{eff} range) and a higher level of mass/age degeneracy. The substellar gap is revealed in the simulated substellar luminosity function with a halo-like birthrate but not in that with a flat birthrate (fig. 10; Burgasser 2004b).

It is important to discover more of these halo brown dwarfs. Deep exploration of the Visible and Infrared Survey Telescope for Astronomy (VISTA; Sutherland et al. 2015) surveys and the future *Euclid* survey (Laureijs et al. 2011) would allow us to identify cooler halo brown dwarfs. The *Euclid* space mission will be particularly well suited to identifying halo brown dwarfs because it will provide NIR slit-less spectra, in addition to its deep optical and *YJH*-band wide-angle imaging. The growing population of known transition-zone brown dwarfs can be used as a benchmark to search for halo brown dwarfs in *Euclid*. Meanwhile, more advanced atmospheric and evolutionary models are required to better understand cool halo brown dwarfs.

REFERENCES

Adams F. C., Bodenheimer P., Laughlin G., 2005, Astron. Nachr., 326, 913
Allard F., Homeier D., Freytag B., 2014, ASInC, 11, 33
Bailer-Jones C. A. L., 2004, A&A, 419, 703
Baraffe I., Chabrier G., Allard F., Hauschildt P. H., 1997, A&A, 327, 1054
Baraffe I., Chabrier G., Barman T. S., Allard F., Hauschildt P. H., 2003, A&A, 402, 701
Baraffe I., Homeier D., Allard F., Chabrier G., 2015, A&A, 577, A42
Basri G., Marcy G. W., Graham J. R., 1996, ApJ, 458, 600
Burgasser A. J., 2004a, ApJ, 614, L73
Burgasser A. J., 2004b, ApJS, 155, 191
Burgasser A. J., Cruz K. L., Kirkpatrick J. D., 2007, ApJ, 657, 494
Burgasser A. J., Vrba F. J., Lépine S., Munn J. A., Luginbuhl C. B., Henden A. A., Guetter H. H., Canzian B. C., 2008, ApJ, 672, 1159
Burgasser A. J., Witte S., Helling C., Sanderson R. E., Bochanski J. J., Hauschildt P. H., 2009, ApJ, 697, 148
Burgasser A. J. et al., 2003, ApJ, 592, 1186
Burrows A., Hubbard W. B., Lunine J. I., Liebert J., 2001, Rev. Mod. Phys., 73, 719
Burrows A. et al., 1998, ASP Conf. Ser. Vol. 134, Advances in the Theory of Brown Dwarfs and Extrasolar Giant Planets. Astron. Soc. Pac., San Francisco, 354
Casali M. et al., 2007, A&A, 467, 777
Cepa J. et al., 2000, Proc. SPIE Vol. 4008, OSIRIS tunable imager and spectrograph. SPIE, Bellingham, 623
Chabrier G., Baraffe I., 1997, A&A, 327, 1039
Chambers K. C. et al., 2016, preprint (arXiv:1612.05560)
Clarke J. R. A. et al., 2010, MNRAS, 402, 575
Cushing M. C., Looper D., Burgasser A. J., Kirkpatrick J. D., Faherty J., Cruz K. L., Sweet A., Sanderson R. E., 2009, ApJ, 696, 986
Delfosse X. et al., 1997, A&A, 327, L25
Dieterich S. B., Henry T. J., Jao W.-C., Winters J. G., Hosey A. D., Riedel A. R., Subasavage J. P., 2014, AJ, 147, 94
Dotter A. et al., 2010, ApJ, 708, 698
Dupuy T. J., Liu M. C., 2017, ApJS, 231, 15
Faherty J. K. et al., 2016, ApJS, 225, 10
Filippazzo J. C., Rice E. L., Faherty J., Cruz K. L., Van Gordon M. M., Looper D. L., 2015, ApJ, 810, 158
Freudling W., Romaniello M., Bramich D. M., Ballester P., Forchi V., García-Dabló C. E., Moehler S., Neeser M. J., 2013, A&A, 559, A96
Hambly N. C. et al., 2008, MNRAS, 384, 637
Hayashi C., Nakano T., 1963, Prog. Theor. Phys., 30, 460
Hewett P. C., Warren S. J., Leggett S. K., Hodgkin S. T., 2006, MNRAS, 367, 454
Hodgkin S. T., Irwin M. J., Hewett P. C., Warren S. J., 2009, MNRAS, 394, 675
Irwin M. J. et al., 2004, Proc. SPIE Vol. 5493, VISTA data flow system: pipeline processing for WFCAM and VISTA. SPIE, Bellingham, 411
Jofré P., Weiss A., 2011, A&A, 533, A59
Kilic M., Munn J. A., Harris H. C., von Hippel T., Liebert J. W., Williams K. A., Jeffery E., DeGennaro S., 2017, ApJ, 837, 162
Kirkpatrick J. D., Allard F., Bida T., Zuckerman B., Becklin E. E., Chabrier G., Baraffe I., 1999, ApJ, 519, 834
Kirkpatrick J. D. et al., 2000, AJ, 120, 447
Kumar S. S., 1963, ApJ, 137, 1121
Laureijs R. et al., 2011, preprint (arXiv:1110.3193)
Lawrence A. et al., 2007, MNRAS, 379, 1599
Line M. R. et al., 2017, ApJ, 848, 83
Lodders K., 1999, ApJ, 519, 793
Lodieu N., Burgasser A. J., Pavlenko Y., Rebolo R., 2015a, A&A, 579, A58
Lodieu N., Espinoza Contreras M., Zapatero Osorio M. R., Solano E., Aberasturi M., Martín E. L., Rodrigo C., 2017, A&A, 598, A92
Lodieu N., Zapatero Osorio M. R., Martín E. L., Solano E., Aberasturi M., 2010, ApJ, 708, L107
Lodieu N., Zapatero Osorio M. R., Rebolo R., Béjar V. J. S., Pavlenko Y., Pérez-Garrido A., 2015b, A&A, 581, A73
Magazzu A., Martin E. L., Rebolo R., 1993, ApJ, 404, L17
Mann A. W., Feiden G. A., Gaidos E., Boyajian T., von Braun K., 2015, ApJ, 804, 64
Martín E. L., Delfosse X., Basri G., Goldman B., Forveille T., Zapatero Osorio M. R., 1999, AJ, 118, 2466
Massey P., Strobel K., Barnes J. V., Anderson E., 1988, ApJ, 328, 315
Oke J. B., 1990, AJ, 99, 1621
Pinfield D. J. et al., 2012, MNRAS, 422, 1922
Rebolo R., Martin E. L., Basri G., Marcy G. W., Zapatero-Osorio M. R., 1996, ApJ, 469, L53
Rebolo R., Martin E. L., Magazzu A., 1992, ApJ, 389, L83
Reddy B. E., Lambert D. L., Allende Prieto C., 2006, MNRAS, 367, 1329
Ruiz M. T., Leggett S. K., Allard F., 1997, ApJ, 491, L107
Shi Y. B., Stancil P. C., Wang J. G., 2013, A&A, 551, A140
Sivarani T., Lépine S., Kembhavi A. K., Gupchup J., 2009, ApJ, 694, L140
Smith L. C. et al., 2018, MNRAS, 474, 1826
Sutherland W. et al., 2015, A&A, 575, A25
Vernet J. et al., 2011, A&A, 536, A105
Weck P. F., Schweitzer A., Kirby K., Hauschildt P. H., Stancil P. C., 2004, ApJ, 613, 567
York D. G. et al., 2000, AJ, 120, 1579
Zhang Z. H., Homeier D., Pinfield D. J., Lodieu N., Jones H. R. A., Allard F., Pavlenko Y. V., 2017b, MNRAS, 468, 261
Zhang Z. H. et al., 2017a, MNRAS, 464, 3040

SUPPORTING INFORMATION

Supplementary data are available at *MNRAS* online.

ULAS_J230711.01+014447.1_xshooter_vis.fits
ULAS_J230711.01+014447.1_xshooter_nir.fits
ULAS_J135058.85+081506.8_xshooter_vis.fits
ULAS_J135058.85+081506.8_xshooter_nir.fits
ULAS_J020858.62+020657.0_xshooter_vis.fits

ULAS_J020858.62+020657.0_xshooter_nir.fits

Please note: Oxford University Press is not responsible for the content or functionality of any supporting materials supplied by the authors. Any queries (other than missing material) should be directed to the corresponding author for the article.

This paper has been typeset from a TEX/LATEX file prepared by the author.